

Mixed-Valence Biferroceniums: Pronounced Effects of Cation–Anion Interactions on the Intramolecular Electron-Transfer Rate

Teng-Yuan Dong,^{*,1} Chun-Hsun Huang,¹ Chung-Kay Chang,¹
Hsing-Ching Hsieh,¹ Shie-Ming Peng,² and Gene-Hsiang Lee²

Department of Chemistry, National Sun Yat-sen University, Kaohsiung, Taiwan, ROC, and
Department of Chemistry, National Taiwan University, Taipei, Taiwan, ROC

Received November 14, 1994[®]

Relatively minor perturbations caused by the cation–anion interactions in 1',2',3',1''',2''',3'''-hexaethylbiferrocenium triiodide (**1**) and 1',2',4',1''',2''',4'''-hexaethylbiferrocenium triiodide (**2**) have pronounced effects on the electronic structure and the rate of intramolecular electron transfer. The X-ray structure of **1** has been determined at 298 K: $P2_1/c$, $a = 9.433(3)$ Å, $b = 18.597(3)$ Å, $c = 10.425(3)$ Å. $\beta = 110.24(2)^\circ$, $Z = 2$, $D_{\text{calcd}} = 1.779$ g cm⁻³, $R_F = 0.037$, and $R_{wF} = 0.035$. The isomeric **2** crystallizes in the monoclinic space group $P2_1/n$ with two molecules in a unit cell with dimensions $a = 12.214(9)$ Å, $b = 11.516(10)$ Å, $c = 12.222(7)$ Å. $\beta = 103.36(5)^\circ$; $R_F = 0.055$, and $R_{wF} = 0.055$. The neutral compound 1',2',3',1''',2''',3'''-hexaethylbiferrocene crystallizes in the triclinic space group $P\bar{1}$ with one molecule in a unit cell with dimensions $a = 7.999(1)$ Å, $b = 8.981(3)$ Å, $c = 11.222(2)$ Å. $\alpha = 112.08(2)^\circ$, $\beta = 76.47(1)^\circ$, $\gamma = 113.80(2)^\circ$; $R_F = 0.027$, and $R_{wF} = 0.032$. The variable-temperature ⁵⁷Fe Mössbauer data indicate that **1** is delocalized on the Mössbauer time scale in the solid state above 170 K. However, the electron-transfer rate in **2** is localized on the Mössbauer time scale at 300 K (electron-transfer rate $< \sim 10^7$ s⁻¹). We suggest that the difference in rates of electron transfer in **1** and **2** is a result of difference in the cation–anion interactions. A comparison of electron-transfer rates in solid state and solution state is also presented.

Introduction

We undertook the present work in the hope that comparison of molecular structures would improve our understanding of the factors that control the rate of intramolecular electron transfer in the solid state for a series of mixed-valence biferrocenium salts. In the solid state, the rate of electron transfer for a given mixed-valence cation is influenced by various structural factors and lattice dynamics,^{3–7} including the electronic and vibronic coupling between two metal ions,^{8–11} the nature of the counterion,^{12–14} and cation–anion interactions.¹⁵ The work to be reported is a refinement and extension

of our earlier preliminary results^{16,17} on the rates of intramolecular electron transfer in a series of alkyl-substituted biferrocenium salts. To further confirm the correlation of structure and rate of electron transfer, we prepared two new mixed-valence polyethylbiferrocenium triiodides (Chart 1; **1** and **2**).

In our original publication,^{11,18} a significant influence on the electron-transfer rate in mixed-valence biferrocenium salt **3** was observed when the cyclopentadienyl (Cp) rings in the ferrocenyl moieties were linked by an interannular trimethylene bridge. We proposed that such a structural modification would lead to increased metal–ligand interactions as the rings tilt. A recent interesting finding is that there is a correlation between the tilt angle and the rate of electron transfer in the series of biferrocenium salts **5–8** and **16**.^{16,17} We proposed a model to explain the difference in the rates of electron transfer of these mixed-valence cations. We suggested that this is a result of difference in the degree of tilting of the Cp rings from a parallel geometry. However, our present physical measurements for **1** and **2** have stimulated us to extend this model to consider characteristics of the cation–anion interactions. Consideration is taken of how the triiodide counterion can interact with the cation to influence the electronic coupling between the Fe centers. In so doing, our new

[®] Abstract published in *Advance ACS Abstracts*, March 1, 1995.

(1) National Sun Yat-sen University.

(2) National Taiwan University.

(3) Cohn, M. J.; Dong, T.-Y.; Hendrickson, D. N.; Geib, S. J.; Rheingold, A. L. *J. Chem. Soc., Chem. Commun.* **1985**, 1095.

(4) Dong, T.-Y.; Hendrickson, D. N.; Iwai, K.; Cohn, M. J.; Rheingold, A. L.; Sano, H.; Motoyama, S. *J. Am. Chem. Soc.* **1985**, *107*, 7996.

(5) Iijima, S.; Saida, R.; Motoyama, I.; Sano, H. *Bull. Chem. Soc. Jpn.* **1981**, *54*, 1375.

(6) Nakashima, S.; Katada, M.; Motoyama, I.; Sano, H. *Bull. Chem. Soc. Jpn.* **1987**, *60*, 2253.

(7) Kai, M.; Katada, M.; Sano, H. *Chem. Lett.* **1988**, 1523.

(8) Dong, T.-Y.; Lee, T. Y.; Lee, S. H.; Lee, G. H.; Peng, S. M. *Organometallics* **1994**, *13*, 2337.

(9) Dong, T.-Y.; Ke, T. J.; Peng, S. M.; Yeh, S. K. *Inorg. Chem.* **1989**, *28*, 2103.

(10) Dong, T.-Y.; Hwang, M. Y.; Wen, Y. S. *J. Organomet. Chem.* **1990**, *391*, 377.

(11) Dong, T.-Y.; Lee, T. Y.; Lin, H. M. *J. Organomet. Chem.* **1992**, *427*, 101.

(12) Dong, T.-Y.; Schei, C. C.; Hsu, T. L.; Lee, S. L.; Li, S. J. *Inorg. Chem.* **1991**, *30*, 2457.

(13) Webb, R. J.; Geib, S. J.; Staley, D. L.; Rheingold, A. L.; Hendrickson, D. N. *J. Am. Chem. Soc.* **1990**, *112*, 5031.

(14) Dong, T.-Y.; Kambara, T.; Hendrickson, D. N. *J. Am. Chem. Soc.* **1986**, *108*, 5857.

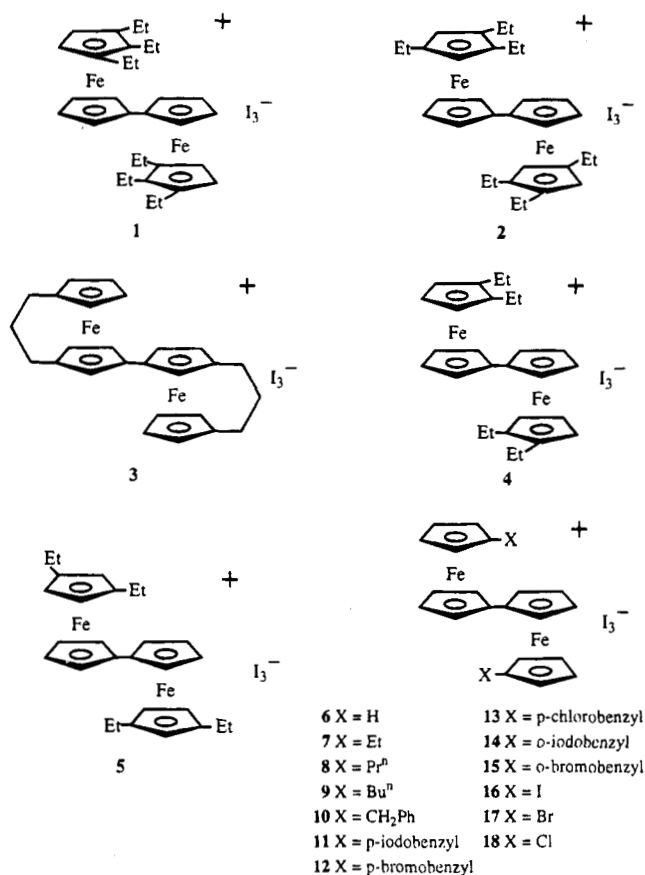
(15) Kambara, T.; Hendrickson, D. N.; Dong, T.-Y.; Cohn, M. J. *J. Chem. Phys.* **1987**, *86*, 2362.

(16) Dong, T.-Y.; Chang, C. K.; Huang, C. H.; Wen, Y. S.; Lee, S. L.; Chen, J. A.; Yeh, W. Y.; Yeh, A. *J. Chem. Soc., Chem. Commun.* **1992**, 526.

(17) Dong, T.-Y.; Huang, C. H.; Chang, C. K.; Wen, Y. S.; Lee, S. L.; Chen, J. A.; Yeh, W. Y.; Yeh, A. *J. Am. Chem. Soc.* **1993**, *115*, 6357.

(18) Dong, T.-Y.; Chou, C. Y. *J. Chem. Soc., Chem. Commun.* **1990**, 1332.

Chart 1



model allows for a more realistic description of the mixed-valence biferrocenium salts 1–18. Our explanation is general and is applicable to other mixed-valence systems. Before the new model is described, the physical properties of 1 and 2 will be presented.

Experimental Section

General Information. The starting materials 1',2'-diethyl-1-bromoferrocene and 1',3'-diethyl-1-bromoferrocene were prepared according to our previous literature procedure.¹⁷ All solvents were dried and distilled under a nitrogen atmosphere. All procedures involving air-sensitive materials were performed under the strict exclusion of air. Chromatography was carried out on neutral alumina (activity II) or silica gel (70–230 mesh).

Acetylation of 1',2'-Diethyl-1-bromoferrocene. The acetylating reagent was prepared according to the Friedel–Crafts synthesis by mixing 0.66 mL (9.7 mmol) of acetyl chloride and excess AlCl₃ in dry CH₂Cl₂ (100 mL) at 0 °C under N₂. The excess of AlCl₃ was filtered off with glass wool.

The acetylating reagent was added by means of a dropping funnel over a period of ~1 h to a solution of 1',2'-diethyl-1-bromoferrocene (2.59 g, 8.1 mmol) in dry CH₂Cl₂ (100 mL) at 0 °C. The mixture was stirred for 4 h at 0 °C and then 1 h at room temperature. The reaction mixture was then poured into an ice–water mixture. The resulting mixture was separated after the reduction of ferrocenium cation with aqueous Na₂S₂O₃. The organic layer was washed with saturated aqueous NaHCO₃ and with water, and then it was dried over MgSO₄. The solvent was removed, and the red oily residue was chromatographed on Al₂O₃. The first band eluted with *n*-hexane–CH₂Cl₂ (7:3) was the starting material. The second band was a mixture of 19 and 20. This mixture could be separated by rechromatographing on silica gel using *n*-hexane–ethyl acetate

(15:1) as the eluent. The first and third bands were 19 (40%) and 20 (15%). The second band was uncharacterized. The physical properties of 19 are as follows. ¹H NMR (CDCl₃, ppm): 1.20 (t, 6H, CH₃), 2.49 (s, 3H, COCH₃), 2.59 (q, 4H, CH₂), 3.96 (t, 2H, Cp), 4.21 (m, 3H, Cp), 4.45 (t, 1H, Cp). Mass spectrum: M⁺ at *m/z* 362.

Reduction of 19. The reduction reaction was carried out by carefully adding, with stirring, small portions of AlCl₃ to a mixture of the ferrocene compound and LiAlH₄ in dry ether. After 30 min, the solution became yellow, an excess of H₂O was added to it, and the ether layer was separated. The ether layer was washed with H₂O and dried over MgSO₄. After the evaporation of the solvent, the crude product was chromatographed on Al₂O₃, eluting with hexane. The first band was the desired compound (21). The yields were ~85%. The physical properties of 21 are as follows. ¹H NMR (CDCl₃, ppm): 1.12 (td, 9H, CH₃), 2.33 (m, 6H, CH₂), 3.85 (t, 2H, Cp), 3.94 (d, 2H, Cp), 4.04 (t, 2H, Cp); mass spectrum: M⁺ at *m/z* 348.

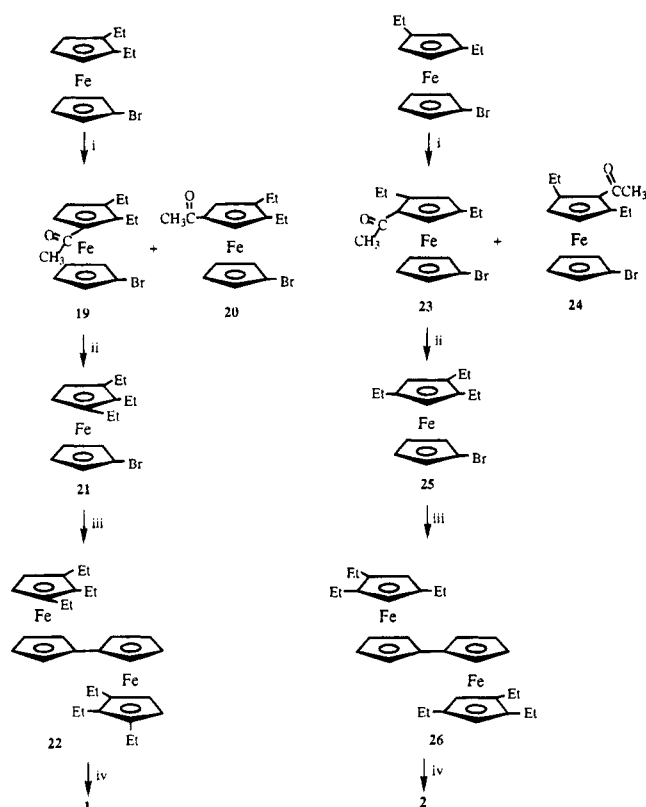
Acetylation of 1',3'-Diethyl-1-bromoferrocene. The Friedel–Crafts reaction of 1',3'-diethyl-1-bromoferrocene was carried out according to the same procedure as the acetylation of 1',2'-diethyl-1-bromoferrocene. The red oily residue was chromatographed on Al₂O₃. The first band eluted with *n*-hexane–CH₂Cl₂ (7:3) was the recovered starting material. The second band was a mixture of 23 and 24. Similarly, this mixture could be separated into three bands by rechromatographing on silica gel using *n*-hexane–ethyl acetate (15:1) as the eluent. The first and third bands were 23 (35%) and 24 (9%), respectively. The second band was uncharacterized. The physical properties of 23 are as follows. ¹H NMR (CDCl₃, ppm): 1.17 (t, 6H, CH₃), 2.37 (s, 3H, COCH₃), 2.61 (m, 4H, CH₂), 3.99 (t, 2H, Cp), 4.03 (t, 2H, Cp), 4.19 (t, 1H, Cp), 4.48 (t, 1H, Cp). Mass spectrum: M⁺ at *m/z* 362.

Reduction of 23. Reduction of 23 with LiAlH₄–AlCl₃ in dry ether was carried out in a manner similar to the reduction of 19. ¹H NMR (CDCl₃, ppm) of 25: 1.27 (t, 9H, CH₃), 2.31 (m, 6H, CH₂), 3.88 (dd, 2H, Cp), 3.94 (d, 2H, Cp), 4.08 (dd, 2H, Cp); mass spectrum: M⁺ at *m/z* 348.

Ullmann Reaction of 21 and 25. Compounds 22 and 26 were prepared by the Ullmann coupling procedure as shown in Scheme 1. A mixture of the corresponding bromoferrocene (1 g) and activated copper (5 g) was heated under N₂ at 110–120 °C for 24 h. After cooling to room temperature, the reaction mixture was repeatedly extracted with CH₂Cl₂ until the CH₂Cl₂ extracts appeared colorless. The extracts were evaporated and chromatographed on neutral Al₂O₃. The first band eluted with hexane yielded starting material. Continued elution with hexane afforded the desired compound. Compounds 22 and 26 were recrystallized from hexane. The yields were ~70%. The physical properties of 22 are as follows: ¹H NMR (CDCl₃, ppm): 1.00 (t, 18H, CH₃), 2.03 (q, 12H, CH₂), 3.74 (s, 4H, Cp), 3.98 (d, 4H, Cp), 4.04 (d, 4H, Cp). mp: 51.5–52.3 °C. Mass spectrum: M⁺ at *m/z* 538. The physical properties of 26 are as follows: ¹H NMR (CDCl₃, ppm): 1.02 (t, 18H, CH₃), 2.08 (q, 12H, CH₂), 3.69 (s, 4H, Cp), 3.93 (d, 4H, Cp), 4.01 (d, 4H, Cp). mp: 40.8–41.5 °C. Mass spectrum: M⁺ at *m/z* 538.

Mixed-Valence Compounds 1 and 2. Crystalline samples of 1 and 2 were prepared by adding a benzene–hexane (1:1) solution containing a stoichiometric amount of iodine to a benzene–hexane (1:1) solution of the corresponding biferrocene at 0 °C. The resulting dark crystals were filtered and washed repeatedly with cold hexane. A more crystalline sample can be prepared by slowly diffusing hexane into a CH₂Cl₂ solution containing the corresponding biferrocenium triiodide salt. Anal. Calcd for 1 (C₃₂H₄₂Fe₂I₃): C, 41.82; H, 4.61. Found: C, 41.47; H, 4.64. Anal. Calcd for 2 (C₃₂H₄₂Fe₂I₃): C, 41.82; H, 4.61. Found: C, 41.55; H, 4.50.

Physical Methods. ⁵⁷Fe Mössbauer measurements were made on a constant-velocity instrument which has been

Scheme 1^a

^a Reagents and conditions: (i) AcCl–AlCl₃; (ii) AlCl₃–LiAlH₄; (iii) activated Cu; (iv) I₂.

previously described.¹⁹ Velocity calibrations were made using a 99.99% pure 10 μm iron foil. Typical line widths for all three pairs of iron lines fell in the range 0.24–0.27 mm s⁻¹. Isomer shifts are reported relative to iron foil at 300 K but are uncorrected for temperature-dependent, second-order Doppler effects. It should be noted that the isomer shifts illustrated in the figures are plotted as experimentally obtained. Tabulated data is provided.

¹H NMR spectra were run on a Bruker AMX500 spectrometer. Mass spectra were obtained with a VG250–70S system. The near-IR spectra were recorded from 2600 to 900 nm in CH₂Cl₂ by using 1.0 cm quartz cells with a Hitachi U-3501 spectrophotometer. The IR spectra were obtained with a Bio-Rad spc3200 spectroscopy.

Electrochemical measurements were carried out with a BAS 100B system. Cyclic voltammetry was performed with a stationary glassy carbon working electrode, which was cleaned after each run. These experiments were carried out with 1 × 10⁻³ M solutions of ferrocene in dry CH₂Cl₂–CH₃CN (1:1) containing 0.1 M of (*n*-C₄H₉)₄NPF₆ as supporting electrolyte. The potentials quoted in this work are relative to a Ag/AgCl electrode at 25 °C. Under these conditions, ferrocene shows a reversible one-electron oxidation wave (*E*_{1/2} = 0.37 V).

Crystal Structure Determinations. The crystals of **1**, **2**, and **22** were mounted, and data were collected on an Enraf-Nonius CAD4 diffractometer at 298 K. Absorption corrections based on ψ -scans for **1**, **2**, and **22** were applied. The structures were solved by the heavy atom method. Positional and anisotropic thermal parameters for non-hydrogen atoms were refined by the full-matrix least-squares method. H atoms were introduced in calculated positions and refined isotropically. Further details are given in Table 1. Atomic positional parameters for **1** are listed in Table 2, and Table 3 contains

Table 1. Experimental and Crystal Data for the X-ray Structures

	1	2	22
formula	C ₃₂ H ₄₂ Fe ₂ I ₃	C ₃₂ H ₄₂ Fe ₂ I ₃	C ₃₂ H ₄₂ Fe ₂
MW	919.08	919.08	538.38
cryst syst	monoclinic	monoclinic	triclinic
space group	<i>P</i> 2 ₁ / <i>c</i>	<i>P</i> 2 ₁ / <i>n</i>	<i>P</i> $\bar{1}$
<i>a</i> , Å	9.433(3)	12.214(9)	7.999(1)
<i>b</i> , Å	18.597(3)	11.516(10)	8.981(3)
<i>c</i> , Å	10.425(3)	12.222(7)	11.222(2)
α , deg			112.08(2)
β , deg	110.24(2)	103.36(5)	76.47(1)
γ , deg			113.80(2)
<i>V</i> , Å ³	1715.9(8)	1672.5(2)	680.4(3)
<i>Z</i>	2	2	1
<i>D</i> _{calcd} , g cm ⁻³	1.779	1.825	1.314
μ , mm ⁻¹	3.54	3.63	1.08
λ , Å	0.709 30	0.709 30	0.709 30
2 θ limits, deg	44.9	44.8	44.8
max, min trans coeff	0.998, 0.895	1.0, 0.716	0.998, 0.852
<i>R</i> _F	0.037	0.055	0.027
<i>R</i> _{wF}	0.035	0.055	0.032

Table 2. Atom Coordinates and Thermal Parameters (Å²) for **1**

	<i>x</i>	<i>y</i>	<i>z</i>	<i>B</i> _{iso} ^a
I1	0.97503(8)	0.88661(4)	0.18346(7)	7.18(4)
I2	1.0	1.0	0.0	5.16(4)
Fe	0.5613(1)	0.03029(6)	0.2862(1)	3.79(6)
C1	0.5123(8)	-0.0196(4)	0.4448(7)	3.2(4)
C2	0.396(1)	-0.0336(5)	0.3178(8)	6.1(5)
C3	0.457(2)	-0.0670(5)	0.234(1)	11(1)
C4	0.611(2)	-0.0773(4)	0.300(1)	10.0(9)
C5	0.651(1)	-0.0451(5)	0.435(1)	6.6(6)
C6	0.7298(8)	0.1029(4)	0.2889(7)	3.6(4)
C7	0.6185(8)	0.1390(3)	0.3301(7)	3.2(4)
C8	0.4746(8)	0.1312(4)	0.2206(7)	3.5(4)
C9	0.5012(9)	0.0921(4)	0.1135(7)	3.9(4)
C10	0.6572(9)	0.0745(4)	0.1568(7)	4.0(4)
C11	0.898(1)	0.0978(5)	0.3679(9)	5.8(5)
C12	0.986(1)	0.1555(6)	0.327(1)	8.0(7)
C13	0.6461(9)	0.1760(4)	0.4636(8)	4.7(5)
C14	0.683(1)	0.2550(5)	0.460(1)	8.4(7)
C15	0.3275(9)	0.1617(5)	0.216(1)	6.0(5)
C16	0.294(1)	0.2346(5)	0.143(1)	9.7(8)

^a *B*_{iso} is the mean of the principal axes of the thermal ellipsoid.

selected bond lengths and angles. Final atomic coordinates for **2** are given in Table 4, with selected bond lengths and angles in Table 3. Final positional and thermal parameters and selected bond lengths and angles for **22** are given in Tables 5 and 3, respectively. Complete tables of interatomic distances and angles and of thermal parameters for these compounds are supplied as supplementary materials.

1',2',3',1''',2''',3''',3''''-Hexaethylbiferrocenium Triiodide (1). A dark needlelike crystal measuring 0.10 × 0.13 × 0.50 mm, grown by layering hexane on a CH₂Cl₂ solution of **1**, was attached to a quartz fiber with hydrocarbon grease. Cell dimensions were obtained from 25 reflections with 23.40° < 2 θ < 27.80°. The θ -2 θ scan technique was used to record the intensities for all reflections for which 1° < 2 θ < 44.9°. Of the 2232 unique reflections, there were 1620 reflections with *F*_o > 2.0 σ (*F*_o²), where σ (*F*_o²) values were estimated from counting statistics. These data were used in the final refinement of structural parameters.

1',2',4',1''',2''',4''',4''''-Hexaethylbiferrocenium Triiodide (2). A dark crystal (0.10 × 0.30 × 0.50 mm) was obtained by following the same procedure as described for **1**. Data were collected to a 2 θ value of 44.8°. The unit cell dimensions were obtained from 25 reflections with 19.80° < 2 θ < 23.18°. Of the 2174 unique reflections, there were 1573 reflections with *F*_o > 2.0 σ (*F*_o²). These data were used in the final refinement of structural parameters.

1',2',3',1''',2''',3''',3''''-Hexaethylbiferrocene (22). An orange

(19) Dong, T.-Y.; Schei, C. C.; Hwang, M. Y.; Lee, T. Y.; Yeh, S. K.; Wen, Y. S. *Organometallics* **1992**, *11*, 573.

Table 3. Selected Bond Distances (Å) and Bond Angles (deg)

	1	2	22
Bond Distances			
I1–I2	2.9106(9)	2.904(2)	
Fe–C1	2.082(7)	2.09(1)	2.069(3)
Fe–C2	2.075(8)	2.07(1)	2.037(3)
Fe–C3	2.04(1)	2.06(1)	2.024(3)
Fe–C4	2.049(8)	2.03(1)	2.044(3)
Fe–C5	2.046(8)	2.05(1)	2.051(3)
Fe–C6	2.079(7)	2.04(1)	2.051(3)
Fe–C7	2.101(7)	2.05(1)	2.045(3)
Fe–C8	2.067(7)	2.05(2)	2.046(3)
Fe–C9	2.044(7)	2.15(2)	2.032(3)
Fe–C10	2.040(7)	2.06(1)	2.033(3)
C1–C1 ^a	1.45(1)	1.44(2)	1.457(6)
C1–C2	1.42(1)	1.43(2)	1.420(4)
C1–C5	1.42(1)	1.43(2)	1.427(4)
C2–C3	1.35(2)	1.44(2)	1.423(5)
C3–C4	1.39(2)	1.38(2)	1.395(7)
C4–C5	1.46(2)	1.40(2)	1.415(5)
C6–C7	1.43(1)	1.48(2)	1.428(4)
C6–C10	1.41(1)	1.42(2)	1.422(4)
C7–C8	1.45(1)	1.38(3)	1.429(4)
C8–C9	1.42(1)	1.34(3)	1.422(5)
C9–C10	1.42(1)	1.50(2)	1.409(5)
Bond Angles			
I2–I1–I2 ^b	180.0	180.0	
C2–C1–C5	107.8(7)	107(1)	106.9(3)
C1–C2–C3	108.9(1)	108(1)	108.9(3)
C2–C3–C4	110(1)	108(1)	108.9(3)
C3–C4–C5	107.3(8)	110(1)	107.7(3)
C1–C5–C4	105.7(9)	108(1)	108.7(3)
C7–C6–C10	108.0(6)	103(1)	107.2(3)
C6–C7–C8	107.5(6)	105(1)	108.6(3)
C7–C8–C9	107.3(6)	119(2)	106.9(3)
C8–C9–C10	108.2(6)	100(2)	108.9(3)
C6–C10–C9	108.8(6)	113(1)	108.4(3)

^a Symmetry equivalents: 1 – x, –y, 1 – z for 1; 1 – x, –y, 1 – z for 2; –x, –y, –z for 22. ^b Symmetry equivalents: 2 – x, 2 – y, –z for 1; 2 – x, –y, –z for 2.

Table 4. Atom Coordinates and Thermal Parameters (Å²) for 2

	x	y	z	B _{iso} ^a
I1	0.8969(1)	0.1202(1)	0.15946(9)	7.70(7)
I2	1.0	0.0	0.0	5.48(7)
Fe	0.6742(2)	0.1087(2)	0.4728(2)	5.7(1)
C1	0.5151(9)	0.035(1)	0.4565(9)	4.6(7)
C2	0.507(1)	0.158(1)	0.446(1)	6.2(8)
C3	0.553(1)	0.192(1)	0.353(1)	6.6(8)
C4	0.590(1)	0.092(1)	0.310(1)	6.4(8)
C5	0.5677(9)	–0.005(1)	0.370(1)	4.9(7)
C6	0.820(1)	0.024(1)	0.543(1)	6.4(8)
C7	0.776(1)	0.087(2)	0.630(1)	8(1)
C8	0.776(1)	0.202(2)	0.599(2)	13(1)
C9	0.811(1)	0.231(2)	0.507(2)	11.9(1)
C10	0.842(1)	0.114(1)	0.472(1)	7.2(9)
C11	0.842(1)	–0.01(2)	0.532(1)	9(1)
C12	0.861(1)	–0.137(1)	0.415(2)	10(1)
C13	0.747(2)	0.034(2)	0.725(2)	14(1)
C14	0.696(2)	0.130(2)	0.799(1)	14(2)
C15	0.814(2)	0.340(2)	0.416(2)	8(2)
C15 ^c	0.827(4)	0.347(3)	0.512(4)	11(3)
C16	0.898(2)	0.385(2)	0.448(2)	18(2)

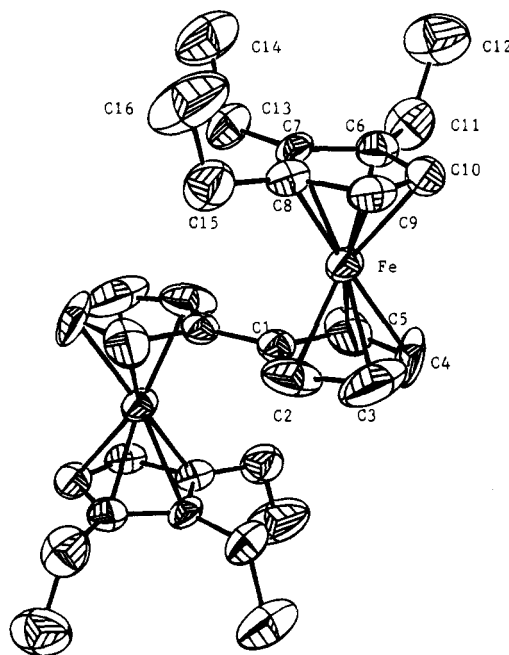
^a B_{iso} is the mean of the principal axes of the thermal ellipsoid.

crystal (0.19 × 0.44 × 0.50 mm), which was grown by slow evaporation from a hexane solution, was used for data collection at 298 K. Cell dimensions were obtained from 20 reflections with 14.70° < 2θ < 32.25°. Data were collected to a 2θ value of 44.8°. The unit cell dimensions were obtained from 25 reflections with 19.80° < 2θ < 23.18°. Of the 1773 unique reflections, there were 1475 reflections with F_o > 2.5 σ (F_o²).

Table 5. Atom Coordinates and Thermal Parameters (Å²) for 22

	x	y	z	B _{iso} ^a
Fe	0.05782(6)	0.11599(5)	0.23969(4)	3.01(2)
C1	–0.0302(4)	–0.0263(4)	0.0578(3)	3.0(1)
C2	0.0498(5)	–0.1109(4)	0.1002(3)	3.9(2)
C3	–0.0529(6)	–0.1383(4)	0.2167(3)	5.1(2)
C4	–0.1932(5)	–0.0715(5)	0.2477(3)	5.3(2)
C5	–0.1801(4)	–0.0011(4)	0.1508(3)	4.1(2)
C6	0.2071(4)	0.3643(4)	0.2433(3)	3.2(2)
C7	0.3247(4)	0.2794(4)	0.2426(3)	3.0(2)
C8	0.2691(4)	0.2225(4)	0.3534(3)	3.4(2)
C9	0.1171(5)	0.2732(4)	0.4216(3)	4.1(2)
C10	0.0785(4)	0.3586(4)	0.3545(3)	3.9(2)
C11	0.2159(5)	0.4489(4)	0.1487(3)	4.5(2)
C12	0.3041(6)	0.6401(5)	0.1969(4)	6.3(3)
C13	0.4823(4)	0.2583(4)	0.1427(3)	4.1(2)
C14	0.6601(5)	0.4106(5)	0.1718(3)	5.2(2)
C15	0.3559(5)	0.1307(4)	0.3932(3)	4.9(2)
C16	0.5128(5)	0.2498(5)	0.4752(4)	5.8(2)

^a B_{iso} is the mean of the principal axes of the thermal ellipsoid.

**Figure 1.** ORTEP drawing of the mixed-valence cation in 1.

Results and Discussion

Structural Studies. X-ray crystallographic studies were undertaken to help us to elucidate the structures and geometric influences on the rate of intramolecular electron transfer. Figures 1–3 display the ORTEP views of the three molecules. They adopt the usual trans conformation as found for most biferrocenium cations and biferrocenes. Only a few cis conformation biferrocenes are known,²⁰ and in all cases, the molecule is held in a cis conformation by a bridge between the 2,2' positions of the fulvalenide ligand. The fulvalenide ligand in 1, 2, and 22 is planar with a crystallographically imposed 0°.

For 1 and 2, the average distances from the iron atom to the two Cp rings are 1.672(5) and 1.676(9) Å, respectively. Furthermore, there is no significant difference between Fe–Cp distance and Fe–fulvalenide distance. In the case of 1, the average Fe–Cp distance

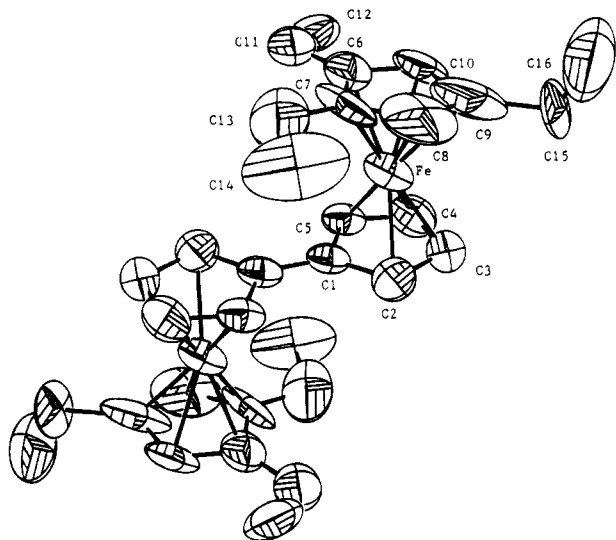


Figure 2. ORTEP drawing of the mixed-valence cation in **2**.

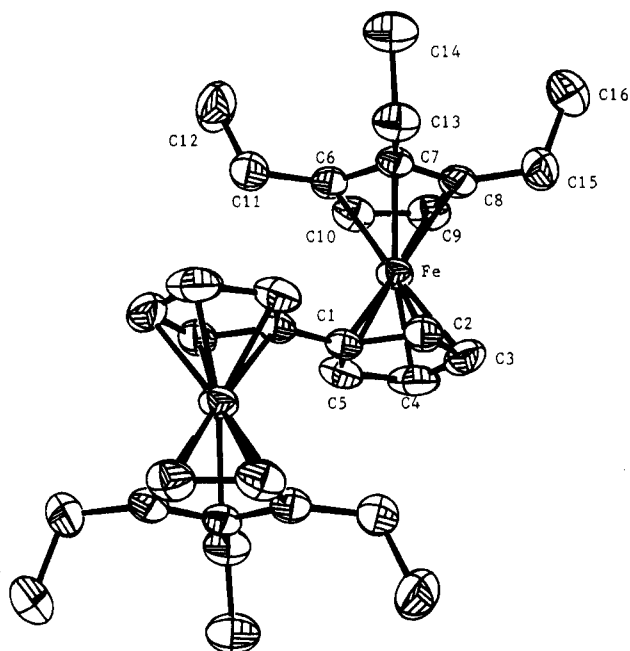


Figure 3. ORTEP drawing of **22**.

(1.672(5) Å) is larger than that for the neutral **22** (1.648(2) Å). Inspection of the Fe–Cp distances in **1** and **2** shows that both distances lie midway between the value of 1.65 Å found²¹ for ferrocene and the value of 1.70 Å found²² for the ferrocenium ion. Mean bond distances from the Fe atom to the rings carbon atoms in **1**, **2**, and **22** are 2.062(8), 2.06(1), and 2.043(3) Å, respectively. Furthermore, the average Fe–C distance in **1** is marginally larger than that in the corresponding neutral biferrocene **22**. The average Fe–C distances in **1** and **2** are very similar, and the values also lie midway between the 2.045 Å observed²¹ for ferrocene and 2.075 Å observed²² for ferrocenium cations. Such an increase in Fe–C and Fe–Cp distances has been observed¹⁹ when ferrocenes are oxidized to the corresponding ferrocenium cations.

The average C–C bond distances in the Cp rings for **1**, **2**, and **22** are 1.42(1), 1.42(1), and 1.419(5) Å, respectively. These values agree well with that in ferrocene (1.42 Å).²¹ The respective dihedral angles between the two least-squares planes of the Cp rings for a given ferrocenyl moiety in **1**, **2**, and **22** are 3.9(4)°, 4.4(7)°, and 1.6(2)°.

The triiodides anions in **1** and **2** are also at the inversion center, showing a symmetric structure. The corresponding I–I bond distances in **1** and **2** are 2.9106(9) and 2.904(2) Å, which are in accord with the accepted value of 2.92 Å reported²³ for the free triiodide ion.

An interesting finding is that the three ethyl substituents on the Cp ring are situated differently. In **1**, the three ethyl substituents are perpendicular to the fulvalenide ligand and this is in contrast to **2**, in which the ethyl substituents stand parallel to the fulvalenide ligand. In both compounds, a three-dimensional hydrogen bonding is clearly found between the Cp hydrogen atoms and the iodine atoms (~3.6 to ~4.1 Å). There is also a hydrogen bond network between ethyl groups and triiodide anions. Consequently, the packing arrangements of the cations and anions in **1** and **2** are different (Figures 4 and 5). In the case of **2**, the packing arrangement can be described as steplike columns. It appears that the parallel ethyl groups on the Cp ring in **2** lead to further slippage of the cations from the steplike stacks seen in **6**–**10**.^{4,24,25} However, the packing arrangement in **1** cannot be described as layer or column structures found in the series of mixed-valence biferrocenium salts **5**–**10**, **12**, **14**, and **16**. In both compounds, there is no Cp–Cp overlap between neighboring cations in the solid-state structure. In the case of **8**, the Cp–Cp interplanar distance is ~3.5 Å and an intermolecular π – π interaction is expected between neighboring cations.

The positioning of the triiodide anion relative to the mixed-valence cation in **2** apparently is also unusual. The triiodide moiety in **2** is parallel to the fulvalenide ligand, rather than perpendicular to the fulvalenide ligand as found in **5**–**9**.^{4,24,25} This type of arrangement is also observed^{19,26} in **10** and **12**. The change of the relative positions of the ethyl substituents from 1',2',4',1''',2''',4''' in **2** to 1',2',3',1''',2''',3''' in **1** leads a dramatic difference in packing arrangement. As shown in Figure 4, **1** is the first mixed-valence biferrocenium salt that contains both parallel and perpendicular fulvalenide–triiodide arrangements.

In our previous papers,^{16,17} we suggested that the degree of tilting of the Cp rings from the parallel geometry plays an important role in determining the rates of electron transfer in the series of mixed-valence biferrocenium salts. However, the deviations of the Cp rings from parallel position were found not to correlate well with the critical temperature for electronic delocalization–localization in the case of mixed-valence biferrocenium salts **1** and **2**. Hence, we suggest that the interactions between cations and anions in **1** and **2**

(23) Runsink, J.; Swen-Walstra, S.; Migchelsen, T. *Acta Crystallogr., Sect. B* **1972**, *28*, 1331.

(24) Konno, M.; Sano, H. *Bull. Chem. Soc. Jpn.* **1988**, *61*, 1455.

(25) Konno, M.; Hyodo, S.; Iijima, S. *Bull. Chem. Soc. Jpn.* **1982**, *55*, 2327.

(26) Webb, R. J.; Dong, T.-Y.; Pierpont, C. G.; Boone, S. R.; Chadha, R. K.; Hendrickson, D. N. *J. Am. Chem. Soc.* **1991**, *113*, 4806.

(21) Seiler, P.; Dunitz, J. D. *Acta Crystallogr., Sect. B* **1979**, *35*, 1068.

(22) Mammano, N. J.; Zalkin, A.; Landers, A.; Rheingold, A. L. *Inorg. Chem.* **1977**, *16*, 297.

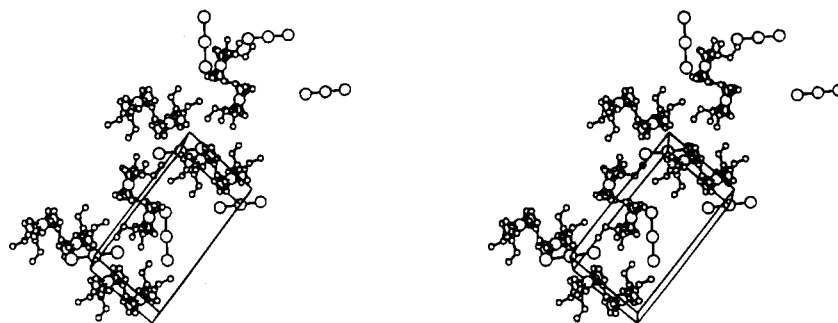


Figure 4. Packing arrangement of 1.

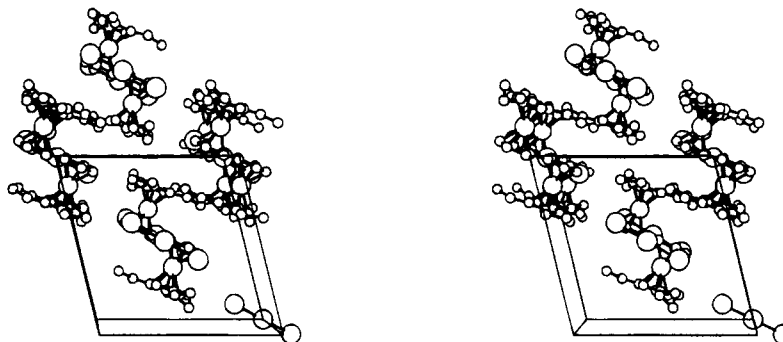


Figure 5. Packing arrangement of 2.

Table 6. Electrochemical Data for Various Biferrocenes

compound	$E_{1/2}^a$ - (V)	$\Delta E_{1/2}^b$ - (V)	ΔmV^c	I_c/I_a^d	$10^{-5} \times K_{com}$
ferrocene	0.37		70	1.02	
biferrocene	0.28	0.31	70	1.01	1.80
	0.59		75	1.01	
1',1'''-diethylbiferrocene	0.20	0.36	68	1.01	12.6
	0.56		70	1.02	
1',2',1''',2'''-tetraethylbiferrocene	0.16	0.37	70	1.13	18.7
	0.53		71	1.01	
1',3',1''',3'''-tetraethylbiferrocene	0.15	0.37	67	0.97	18.7
	0.52		65	1.02	
22	0.17	0.38	70	1.27	27.6
	0.55		70	1.02	
26	0.15	0.38	74	1.00	27.6
	0.53		63	1.07	

^a All half-wave potentials are referred to the AgCl/Ag electrode. ^b Peak separation between two waves. ^c Peak-to-peak separation between the resolved reduction and oxidation wave maxima. ^d Peak-current ratio between cathode and anode.

can also have a pronounced impact on the rate of intramolecular electron transfer. In other words, the positioning of the triiodide anion relative to the mixed-valence cation plays an important role in determining the rate of electron transfer. We suggest that the hydrogen bond networks between the alkyl substituent and the triiodide anion in the series of mixed-valence biferrocenium salts play a crucial role in controlling the magnitude of cation-anion interactions and the degree of tilting of the Cp rings from parallel geometry. A detailed discussion of the effects of structural characteristics on the rate of intramolecular electron transfer in mixed-valence biferrocenium salt will be presented in the later section.

Electrochemical Results. Electrochemical data for **22** and **26**, as well as those for some other relevant compounds, are shown in Table 6. As shown in Figure 6, the neutral compounds **22** and **26** undergo two successive reversible one-electron oxidations to yield the mono and then the dication. Electrochemical revers-

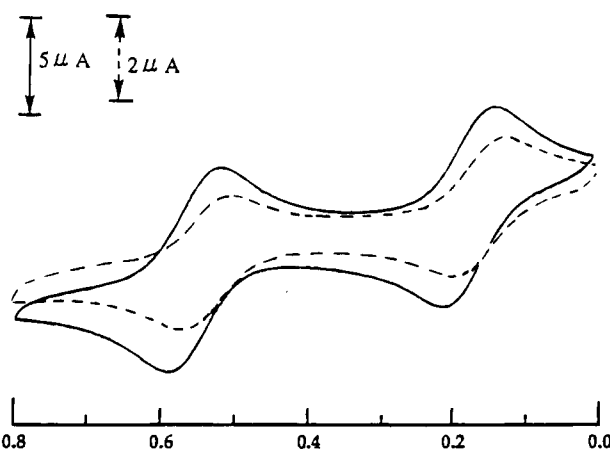


Figure 6. Cyclic voltammograms of **22** (—) and **26** (---); $\nu = 100 \text{ mV s}^{-1}$.

ibility was demonstrated by the peak-to-peak separation between the resolved reduction and oxidation wave maxima.

The effect of ethyl substituents on the stability of the Fe(III) state is illustrated by the shift of half-wave potentials. In a general way, electron-donating groups stabilize the ferrocenium cation, lowering the half-wave potential, and electron-withdrawing groups have the opposite effect. The comparison of the half-wave potentials of ethyl biferrocene with that of biferrocene indicates that the ethyl group clearly acts as a net electron donor. However, it is clear that the electronic effect of the ethyl substituent on half-wave potential is not additive. Hence, an extra ethyl substituent on the Cp ring of **22** and **26** does not lower the half-wave potentials in comparison with 1',2',1''',2'''-tetraethylbiferrocene or 1',3',1''',3'''-tetraethylbiferrocene.

It has been shown that the magnitude of the peak-to-peak separation ($\Delta E_{1/2}$) gives an indication of the interaction through the fulvalenide bridge between the

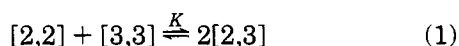
Table 7. Absorption Maximum of IT Band and Activation Parameters

compd	ν_{\max}^a	ϵ_{\max}^b	$\Delta\nu_{1/2(\text{obsd})}^a$	$\Delta\nu_{1/2(\text{calcd})}^a$	α^2	H_{ab}	$10^{-12} \times K_{\text{et}}$
6	4878	958	3384	3357	0.0108	508	1.55
7	5035	1104	2892	3410	0.0103	512	1.29
4	5000	1089	2602	3398	0.0092	480	1.19
5	5120	1163	2483	3439	0.0092	491	1.06
1	5074	1173	2397	3424	0.0090	482	1.09
2	5074	1197	2282	3424	0.0088	475	1.06

^a In cm^{-1} . ^b In $\text{M}^{-1} \text{cm}^{-1}$.

two Fe sites.²⁷ A comparison of the magnitude of $\Delta E_{1/2}$ for various ethyl-substituted biferrocenes indicates that the magnitude of interaction between the two Fe sites in these compounds is similar. However, a comparison of the $\Delta E_{1/2}$ values for ethyl-substituted biferrocenes with that for biferrocene indicates that the interaction between the two Fe sites in ethyl-substituted biferrocene is larger than that in biferrocene.

Coulometry experiments show that each of the two waves is a one-electron-transfer process. In eq 1, the



abbreviation [3,3] denotes the dioxidized cation, [2,3] the monooxidized cation, and [2,2] the neutral compound. Comproportionation equilibrium constants K for various biferrocenes are shown in Table 6. In the studies of electron-transfer rate in the solution state, quantitative calculations based on the concentration of [2,3] have been corrected for this equilibrium.

Electron Transfer in the Solution State. Mixed-valence compounds **1**, **2**, and **4–7** exhibit an IT band at $\sim 5000 \text{ cm}^{-1}$ in the near-IR absorption spectrum. An intervalence transition (IT band) has been defined as metal-to-metal charge transfer. A description of the width of the IT band, the extent of electron delocalization, and the electron-transfer properties of mixed-valence dimers has been given by Hush.²⁸ This work is based on Hush's electron-transfer model. Hush derived an expression for the bandwidth (in cm^{-1}) at half-maximum of the IT band of a localized, homonuclear mixed-valence dimer at 300 K as

$$\Delta\nu_{1/2} = [2310\nu_{\max}]^{1/2} \quad (2)$$

where ν_{\max} is the frequency (in cm^{-1}) of the absorption maximum. The absorption maximum of IT bands in the series of mixed-valence biferrocenium and activation parameters calculated were collected in Table 7. An interesting finding is that the IT bands of ethyl-substituted biferrocenium cations are all sharper than what is expected on the basis of eq 2. An agreement, to about $\sim 10\%$, between $\Delta\nu_{1/2(\text{calcd})}$ and $\Delta\nu_{1/2(\text{obsd})}$ is usually taken as an indication that the Hush model is a satisfactory description of a localized mixed-valence system. In the case of **6**, a good agreement is observed. For localized dimers, the IT bands tend to be very broad and symmetrical, whereas the delocalized dimers have narrower profiles that are asymmetric broader on the blue side than on the red side.²⁸ For example, the IT band in the delocalized Creutz-Taube ion is ~ 6 times

sharper than that predicted by eq 2.²⁹ The Hush model is derived for the high-temperature limit, the criterion for that limit being $2RT > h\nu$, where $h\nu$ is the energy associated with a metal–ligand vibrational transition. It is possible that we are not at the high-temperature limit for either a Fe(II)–Cp or a Fe(III)–Cp vibration in ethyl-substituted biferrocenium cation. Owing to the ethyl substituent, the Fe–Cp vibrational energy in **1**, **2**, **4**, **5**, and **7** is higher than that in **6**. Possibly as a consequence of this fact, Hush's correlation of band energy with bandwidth (at room temperature, eq 2) fails.

The extent of electron delocalization for a given mixed-valence biferrocenium cation can be calculated from eq 3. The average value (5.1 Å) of Fe–Fe distances

$$\alpha^2 = \{4.24 \times 10^{-4} \epsilon_{\max}(\Delta\nu_{1/2})\} / \{\nu_{\max} d^2\} \quad (3)$$

in a series of dialkyl mixed-valence biferrocenium cation is used as donor–acceptor distance.^{4,24,30} In this man-

$$H_{\text{ab}} = \nu_{\max} \alpha \quad (4)$$

$$K_{\text{et}} = \nu_{\text{et}} \exp(-\nu_{\max}/4K_{\text{B}}T) \quad (5)$$

$$\nu_{\text{et}} = (2\pi/\hbar) H_{\text{ab}}^2 (\pi/K_{\text{B}}T\nu_{\max})^{1/2}$$

ner, the values of α^2 for the series of biferrocenium cations were obtained and collected in Table 7. As shown in Table 7, it can be concluded that these biferrocenium cations are examples of class II mixed-valence compounds.^{31,32}

The magnitude of the electronic coupling can be estimated by using eq 4. Finally, the rate constant (K_{et}) of intramolecular electron transfer can be calculated from eq 5, where ν_{et} is the hopping frequency. From the rate constants illustrated in Table 7, the electron-transfer rates in the series of ethyl-substituted biferrocenium cations are quite similar. This similarity in rate clearly indicates that the extra ethyl substituent in **1**, **2**, **4**, and **5** does not play an important role in determining the rate of electron transfer in solution state. This is in agreement with the electrochemical measurement.

⁵⁷Fe Mössbauer Characteristics. The dependence of sample history in Mössbauer spectra has been noted for a few mixed-valence biferrocenium salts.⁴ To examine this phenomenon more thoroughly, we prepared samples of **1** and **2** by two different methods as described in the Experimental Section. In our case, the samples prepared by two different methods gave essentially identical variable-temperature ⁵⁷Fe Mössbauer spectra. Some of these spectra for mixed-valence **1** are illustrated in Figure 7 and fitting parameters are collected in Table 8. The examination of these spectra shows that in the 77–170 K region **1** is converting from valence trapped to valence detrapped and this process is completed by 170 K. The features in the low-temperature Mössbauer spectrum are two doublets, one for an Fe(III) site and the other for an Fe(II) site. Both

(29) Creutz, C.; Taube, H. *J. Am. Chem. Soc.* **1973**, *95*, 1086.

(30) Webb, R. J.; Rheingold, A. L.; Geib, S. J.; Staley, D. L.; Hendrickson, D. N. *Angew. Chem., Int. Ed. Engl.* **1989**, *28*, 1388.

(31) Brown, D. B., Ed. *Mixed-Valence Compounds, Theory and Applications in Chemistry, Physics, Geology and Biology*; Reidel Publishing Co.: Boston, MA, 1980.

(32) Day, P. *Int. Rev. Phys. Chem.* **1981**, *1*, 149.

(27) Morrison, W. H. Jr.; Krogsrud, S.; Hendrickson, D. N. *Inorg. Chem.* **1973**, *12*, 1998.

(28) Hush, N. S. *Prog. Inorg. Chem.* **1967**, *8*, 391.

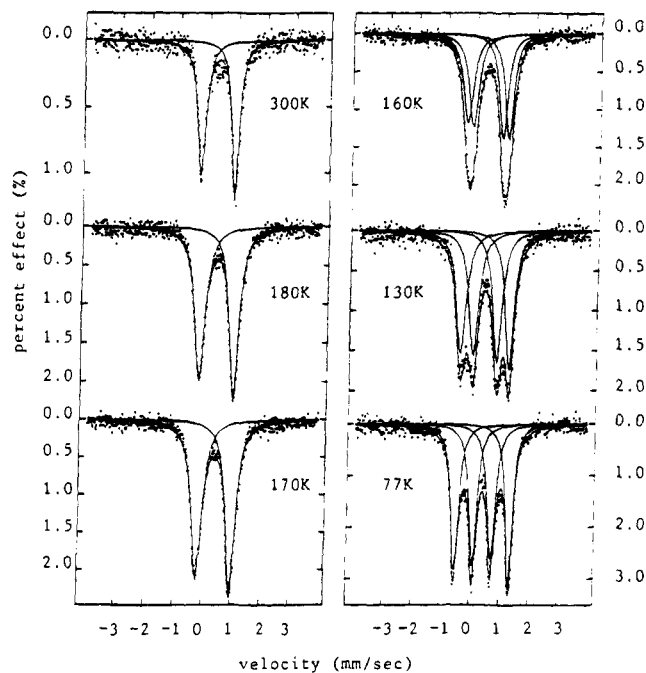


Figure 7. Variable-temperature ^{57}Fe Mössbauer spectra of **1**.

Table 8. ^{57}Fe Mössbauer Least-Squares-Fitting Parameters

compd	T (K)	ΔE_Q^a	δ^b	Γ^c
1	300	1.179	0.441	0.352, 0.297
	180	1.196	0.492	0.442, 0.389
	170	1.179	0.493	0.448, 0.400
	160	1.401	0.506	0.398, 0.351
		1.012	0.500	0.417, 0.349
		1.658	0.513	0.400, 0.378
2	130	0.813	0.507	0.406, 0.359
	77	1.868	0.509	0.339, 0.323
		0.627	0.510	0.314, 0.287
2	300	2.039	0.406	0.286, 0.290
		0.522	0.412	0.432, 0.395
	77	2.031	0.405	0.283, 0.286
		0.521	0.411	0.429, 0.392

^a Quadrupole splitting (in mm s^{-1}). ^b Isomer shift referred to iron foil (in mm s^{-1}). ^c Full width at half-height taken from the least-squares-fitting program. The width for the line at more positive velocity is listed first for the doublet.

doublets have the same area. This pattern of two doublets is what is expected for a mixed-valence biferrocenium cation that is valence trapped on the Mössbauer time scale ($\sim 10^7 \text{ s}^{-1}$). At temperatures above 170 K, the spectrum of this sample shows a single quadrupole-split doublet which is characteristic of a valence-detraped cation in which the electron-transfer rate exceeds $\sim 10^7 \text{ s}^{-1}$. At 170 K, the valence-detraped doublet has $\Delta E_Q = 1.179 \text{ mm s}^{-1}$. There is one interesting aspects of the temperature dependence of the Mössbauer spectra shown in Figure 7. The two valence-trapped doublets at low-temperature Mössbauer spectrum just move together as the temperature is increased. There is very little line broadening evident in the averaging process. Absence of line broadening in variable-temperature Mössbauer spectra has been noted^{3,4,33} for a few mixed-valence biferrocenium salts. A description of this averaging process will be given in a later section.

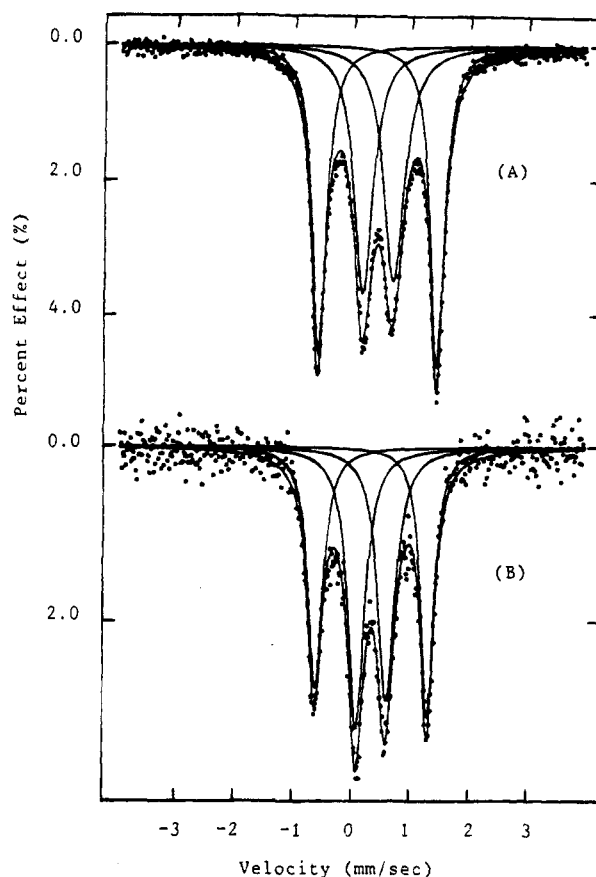


Figure 8. ^{57}Fe Mössbauer spectra of **2** at 300 (A) and 77 K (B).

^{57}Fe Mössbauer spectra were collected at 77 and 300 K for **2**. As shown in Figure 8, this mixed-valence compound shows two doublets in the 300 K Mössbauer spectrum shows two doublets in the 300 K Mössbauer spectrum (Fe(II) site, $\Delta E_Q = 2.039 \text{ mm s}^{-1}$; Fe(III) site, $\Delta E_Q = 0.522 \text{ mm s}^{-1}$). This pattern is expected for a mixed-valence cation that is valence trapped on the time scale of the Mössbauer technique (electron-transfer rate $< \sim 10^7 \text{ s}^{-1}$).

The Mössbauer results indicate that the change of the relative positions of the ethyl substituents from 1',2',3',1''',2''',3''' in **1** to 1',2',4',1''',2''',4''' in **2** leads to a reduction in the intramolecular electron-transfer rate. We believe that this difference in rate is not only due to a difference in electronic and steric effects of the ethyl substituents. First, it is clear that the electronic effect of the ethyl substituent is not additive by comparing the transition temperatures of **1**, **2**, **4**,^{16,17} **5**, **6**,^{3,4} and **7**: 170, >300, 195, 125, >300, and 275 K, respectively. In the comparison of the transition temperature of **1** or **2** with **5**, an extra ethyl substituent on the Cp ring of **1** or **2** does not increase the rate of electron transfer. Instead, the rates of electron transfer in **1** and **2** are decreased. Similarly, the electron-transfer rate in **1** is also slower than that in **5**. However, an extra ethyl substituent on the Cp ring of **4** and **5** does increase the rate of electron transfer, as shown by a comparison of the transition temperature of **4** and **5** with **7**. Further evidence can be gleaned from the electrochemical data of neutral ethylbiferrocenes. These compounds show two one-electron oxidation waves (Table 6). It has been shown that the peak-to-peak separation ($\Delta E_{1/2}$) can gauge the interaction between two Fe sites. As shown in Table 6, the magnitudes of the electronic interactions

(33) Dong, T.-Y.; Cohn, M. J.; Hendrickson, D. N.; Pierpont, C. G. *J. Am. Chem. Soc.* **1985**, *107*, 4777.

between the two Fe atoms in ethylbiferrocenes are nearly equivalent.

Second, it is possible that the relative position of ethyl substituents on a given Cp ring plays an interesting role in controlling the rate of electron transfer in the solid state. The rate of electron transfer will be increased if two ethyl substituents are relative in meta position. The Mössbauer results indicate that the electron-transfer rate in 1',3',1''',3''''-tetraethylbiferrocenium triiodide (**5**) is faster than that in 1',2',1''',2''''-tetraethylbiferrocenium triiodide (**4**).^{16,17} Similarly, in **2** there are two pairs of ethyl substituents in the meta position. Consequently, the rate of electron transfer in **2** is faster than that in **1**.

We suggest that the difference in rates of electron transfer in the series of ethylbiferrocenium cations is a result of structural difference in the solid state. We believe that the magnitude of cation-anion interaction and the Cp ring tilting in the ferrocenyl moiety play a crucial role in intramolecular electron transfer in the biferrocenium system. The ethyl substituents on the Cp ring modify the local structure of the biferrocenium cation and lead to a difference of electron-transfer rate. More detailed discussion will be presented in a later section.

IR Spectroscopy. IR spectroscopy has proven to be useful to tell whether a given mixed-valence biferrocenium cation is delocalized or not.^{4,33} When Fe(II) metallocene is oxidized to Fe(III) metallocene, there is a dramatic change in the IR spectrum. It has been shown that the perpendicular C-H bending band is the best diagnosis of the oxidation state. This band is seen at 815 cm⁻¹ for ferrocene and at 851 cm⁻¹ for ferrocenium triiodide. Mixed-valence biferrocenium cations that have a negligible potential energy barrier for electron transfer should exhibit one C-H bending mode for the Fe(II) moiety and one for the Fe(III) moiety.

Infrared spectra were run for KBr pellets of **1** and **2**. In **1**, for the perpendicular C-H bending region there are relatively strong bands at 820 and 834 cm⁻¹. Similarly, there are C-H bending bands at 818 and 839 cm⁻¹ for **2**. It is clear that, on the IR time scale, the mixed-valence cations **1** and **2** have both Fe(II) and Fe(III) moieties. In other words, the electron-transfer rates in the cations of **1** and **2** are less than $\sim 10^{12}$ s⁻¹ at 300 K.

Factors in Controlling the Rate of Electron Transfer in the Solid State. The goal of this section is to present an explanation for the differences of electron-transfer rates in the series of mixed-valence biferrocenium cations.

In the last few years there has been considerable progress made in understanding what factors control the rate of intramolecular electron transfer in the solid state for mixed-valence biferrocenium salts.^{4,13-19,34-37} Three different types of temperature dependencies have been observed in a series of various disubstituted biferrocenium triiodide compounds. There are those that are valence trapped at all temperatures, those that

are valence detrapped at all temperatures, and those that are valence trapped at low temperature to valence detrapped at some higher temperatures with no discernible line broadening in the averaging process. If intramolecular electron transfer for a biferrocenium cation were slow on the Mössbauer time scale (rate $< \sim 10^7$ s⁻¹) at low temperature and then increased with increasing temperature, the rate should go through the range where coalescence effects would be seen. The line widths of Fe(II) and Fe(III) doublets would be expected to broaden as the electron-transfer rate goes through the ⁵⁷Fe Mössbauer window ($\sim 10^7$ s⁻¹). This is not seen for mixed-valence compounds **1** and **2**. Hendrickson suggested^{4,13,15} that what is affecting the Mössbauer spectrum and imparting a temperature dependence is the onset of lattice dynamics (a second-order phase transition). As the temperature of a compound is increased, the thermal energy could achieve the value necessary to trigger off a cooperative change in the crystal lattice. In Hendrickson's theoretical model,¹⁵ the factors that are potentially important in controlling the rate of intramolecular electron transfer in a mixed-valence biferrocenium cation include the effective barrier for charge oscillation in the anion and the intermolecular cation-cation and cation-anion interactions. It is possible that the onset of vibrational motion involving the I₃⁻ counterion controls the rate of electron transfer in mixed-valence biferrocenium triiodide salts. When the I₃⁻ counterion is thermally activated, it interconverts between two configurations, I_a-I_b-I_c and I_a-I_b-I_c⁻. In each of these limiting forms the two iodine-iodine bond lengths are not equal. The oscillatory charge motion associated with it controls whether charge can be pulled back and forth in the mixed-valence cation.

In our previous paper,¹⁷ we found that the deviations of the Cp rings from the parallel position correlate quite well with the Mössbauer critical temperature for electronic delocalization-localization in mixed-valence biferrocenium salts. The Cp tilt angles in each ferrocenyl moiety for **6**, **7**, **5**, and **16** are 0.3, 4.8, 5.9 and 15.6°, respectively. The transition temperatures from localized to delocalized states on the Mössbauer time scale for **6**, **7**, **5**, and **16** are 365, 275, 125, and <4.2 K, respectively. In our previous paper,¹⁷ we also found that the HOMO-LUMO gap in biferrocenium cation decreases as the tilt angle increase. Bending back the Cp rings leads to a larger extent of metal-ligand interactions. We found that the metal nonbonding orbitals (d_{x²-y²}, d_{xy}) start to interact with ligand π orbitals. Here, the question is to have a reasonable explanation for the difference of electron-transfer rates in new mixed-valence compounds **1** and **2**. The tilt angles of the two Cp rings in the ferrocenyl moiety for **1** and **2** are 3.9° and 4.4°, respectively. The respective Mössbauer localized-delocalized transition temperatures for **1** and **2** are 170 and >300 K. Thus, it cannot fit into the correlation of tilt angle with electron-transfer rate. We believe that the cation-anion interaction in **1** and **2** plays a predominant role in determining the electron-transfer rate. We suggest that the deviation of the correlation results from the difference of packing arrangements for triiodide anions. As discussed in the X-ray section, one of the triiodide anions in **1** is perpendicular to the fulvalenide ligand, not parallel to the fulvalenide ligand

(34) Dong, T.-Y.; Hendrickson, D. N.; Pierpont, C. G.; Moore, M. F. *J. Am. Chem. Soc.* **1986**, *108*, 963.

(35) Moore, M. F.; Wilson, S. R.; Cohn, M. J.; Dong, T.-Y.; Mueller-Westerhoff, U. T.; Hendrickson, D. N. *Inorg. Chem.* **1985**, *24*, 4559.

(36) Dong, T.-Y.; Kambara, T.; Hendrickson, D. N. *J. Am. Chem. Soc.* **1986**, *108*, 4423.

(37) Sorai, M.; Nishimori, A.; Hendrickson, D. N.; Dong, T.-Y.; Cohn, M. J. *J. Am. Chem. Soc.* **1987**, *109*, 4266.

as found in **2**. In other words, the charge oscillation of the I_3^- anion in **1** is parallel to the electron-transfer pathway and this leads to a stronger ability to pull the charge back and forth in the mixed-valence cation. Furthermore, the impact of relative cation–anion position on the electron-transfer rate can be also applied to the case of **12** and **14** reported in our previous paper.¹⁹ The I_3^- moiety in **12** is parallel to the fulvalenide ligand rather than perpendicular to the fulvalenide ligand as found in **14**. Thus, **14** has a faster electron-transfer rate than **12**. The critical transition temperatures of **12** and **14** in variable-temperature Mössbauer studies are 200 and <77 K, respectively.

Comparison of Electron-Transfer Rate in Solid and Solution States. Mössbauer spectra indicating the presence of localized electronic structure at 300 K have been observed for **2** in the solid state. In the studies of variable-temperature Mössbauer technique, **1** converts from valence trapped to valence detrapped and this process is completed by 170 K. The energy and the line shape of the IT band clearly indicate that the intramolecular electron-transfer rates in **1** and **2** in solution are greater than in the solid state. In the solid state, the rate of electron transfer for a given mixed-valence cation is influenced by various structural factors

and lattice dynamics, including the electronic and vibronic couplings between two metal ions, the nature of the counterion, and cation–anion interactions. In general, the electron-transfer rate for a given mixed-valence biferrocenium cation in the solution state is greater than that in the solid state. In the solid state, we have demonstrated that relatively minor perturbations caused by interactions between neighboring cations and anions have pronounced effects on electron transfer. In solution, the manner in which the mixed-valence cation is solvated also influences the rate of intramolecular electron transfer. If ion pairing is present, the anion must move rapidly so as not to limit the rate of intramolecular electron transfer.

Acknowledgment. Our work was generously supported by the National Science Council (NSC84-2113-M-110-015) and National Sun Yat-sen University. We gratefully acknowledge this support.

Supplementary Material Available: Complete tables of positional parameters, bond lengths and angles, and thermal parameters for **1**, **2**, and **22** (23 pages). Ordering information is given on any current masthead page.

OM940860M